NUCLEAR SCIENCE AND TECHNIQUES **25**, 060203 (2014)

Imaging principle and experiment results of an 11 MeV low-energy proton radiography system*

LI Yi-Ding (李一丁),[1,†] ZHANG Xiao-Ding (张小丁),[1] WEI Tao (魏涛),[1] ZHAO Liang-Chao (赵良超),[1]
HE Xiao-Zhong (何小中),[1] MA Chao-Fan (马超凡),[1] YANG Guo-Jun (杨国君),[1] and JIANG Xiao-Guo (江孝国)[1]

[1]*Institute of Fluid Physics, CAEP, P. O. Box 919-106, Mianyang 621900, China*

(Received January 2, 2014; accepted in revised form June 19, 2014; published online December 9, 2014)

Differing from radiography without lens system, the high-energy proton radiography (PRAD) uses Zumbro lens system to focus the penetrating protons. Since the Zumbro lens system is able to limit the range of multiple Coulomb scattering angles of the protons, the low-energy PRAD with Zumbro lens system is also feasible, although the attenuation of probing protons in the object is negligible. Low-energy PRAD is superior to the high-energy PRAD for diagnosing the objects of small thicknesses. To verify the imaging principle of Zumbro lens system, 11 MeV PRAD experiments were performed at the China Academy of Engineering Physics (CAEP) recently. The experiment results demonstrated that this 11 MeV PRAD was able to radiograph objects of area density less than 2.7×10^{-2} g/cm^2 and the area density discrepancy less than 2.3% could be distinguished.

Keywords: Proton radiography, Multiple coulomb scattering, Zumbro lens system, Radiation length, Fourier plane

DOI: 10.13538/j.1001-8042/nst.25.060203

I. INTRODUCTION

Radiography, as an imaging technique, uses radiation to diagnose internal structure of an object under study. A classical radiography system uses X-rays to transmit through an object to a detector plane to obtain a shadow-graph of the object. The idea to use protons in radiograph was first investigated in 1960s [1]. However, unlike X-rays, the probing protons undergo multiple Coulomb scattering (MCS) while passing through an object, and the radiographic image blurs since a proton does not travel in a straight line in the object. The detector should be placed immediately downstream of the object to reduce transverse displacement while the protons travel from the object to the detector.

In 1990s, scientists at Los Alamos National Laboratory (LANL) investigated the high-energy proton radiography (PRAD) as a new tool for advanced hydrotesting. Due to the long attenuation length of high-energy protons, the high-energy PRAD is suited for diagnosing thick objects. To compensate the MCS angles of protons, a magnetic lens system called Zumbro lens system [2] was used in high-energy PRAD to focus the protons leaving the object on a distant image plane. The spatial resolution was well improved as the image blur caused by MCS is eliminated.

The 800 MeV and 24 GeV high-energy PRAD experiments performed with Zumbro lens system at the Los Alamos Neutron Scattering Center (LANSCE) and the Alternating Gradient Synchrotron (AGS), USA [3, 4] proved that it can provide multiple detailed radiographs (spatial resolution better than 1 mm) of fast succession (~ 200 ns between frames) in thick systems, and is superior to X-ray radiography for advanced hydrotesting [5].

In Russia, a 70 GeV PRAD beamline was built on the U-70 accelerator at Institute of High Energy Physics (IHEP) [6] to perform static and dynamic experiments.

For developing high-energy PRAD in China, we built a PRAD beamline of Zumbro lens system at CAEP (China Academy of Engineering Physics) to verify the imaging technique [7], using 11 MeV proton beams from a cyclotron [8], as high-energy proton accelerators are not available in China. At such a low-energy, energy-loss of the protons traversing a thick object would bring with considerable energy dispersion and chromatic aberration. Thus, thickness of the object to be radiographed is limited to reduce the energy-loss. The object was orders of magnitude thinner than the proton attenuation length, so that attenuation of the protons traversing the object was negligible. Theoretical analysis shows that the 11 MeV low-energy PRAD can provide a graph with contrast of different object thicknesses. Also, PRAD experiments on an aluminum foil verified the two primary features of Zumbro lens system: the point-to-point focus from object to image and the forming of a Fourier plane where the protons were sorted by the magnitude of scattering in the object.

II. HIGH-ENERGY PRAD USING ZUMBRO LENS SYSTEM

A PRAD system is shown schematically in Fig. 1. Proton beams extracted from the accelerator are transferred to the object by a matching section, in which the proton beams are diffused and modulated. The protons penetrating the object are focused by the Zumbro lens system onto the scintillator plate, which collects the protons and scintillates. The CCD camera takes pictures of the scintillator to get the radiographic image.

The Zumbro lens system is composed by four magnetic quadrupoles. The object to be radiographed and the scintillator plate are respectively placed at the object and image planes of this lens system. The transverse transfer matrix of the Zumbro lens system is minus-identity ($-I$), thus protons exiting each point of the object are focused onto the scintillator plate (Fig. 2). Owing to this point-to-point focus, transverse

* Supported by National Natural Science Foundation of China (Nos. 11205144 and 11176001)
† Corresponding author, liyd@mail.ustc.edu.cn

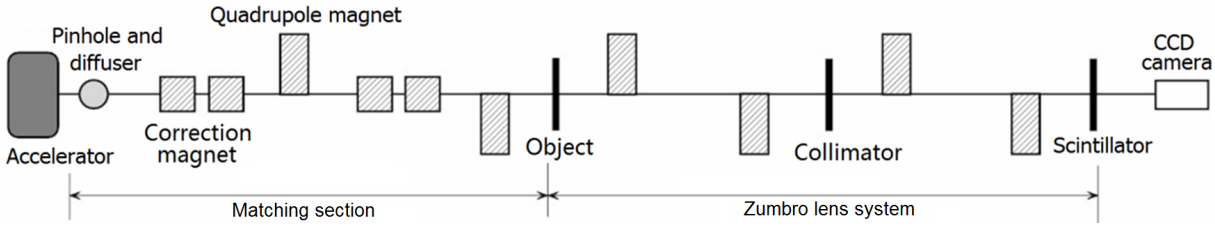

Fig. 1. Layout of the imaging beamline.

distribution of the protons exiting the object can be repeated at the image plane and a 1:1 inverted image of the object can be recorded by the CCD camera. Transverse positions of the protons arriving at the image plane are independent of their initial scattering angles at the object plane, so the angular dispersion caused by MCS will not blur the radiographic image.

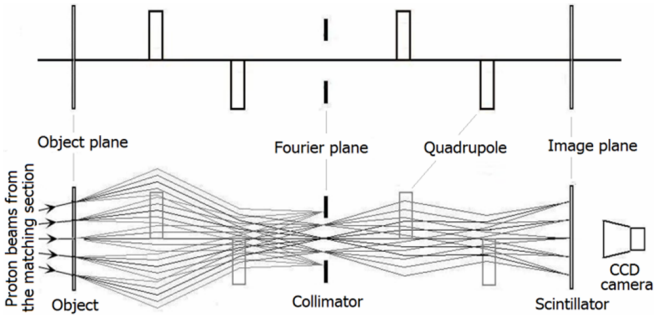

Fig. 2. Schematic of the Zumbro lens system and the proton trajectories.

The design of Zumbro lens system has another feature: at the Fourier plane, of the gap between the two middle quadrupoles, the protons are sorted by their MCS scattering angles in the object, regardless of which point in the object plane they originated from. The MCS changes transverse angle of a proton passing through the object by a deviation angle θ (Fig. 3), which determines radial distance of the proton when it arrives at the Fourier plane. Placing a collimator at the plane can make cuts on the MCS deviation angles of the passing through protons (Fig. 2).

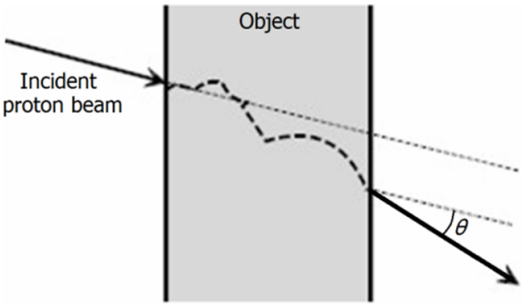

Fig. 3. Trajectory of a proton traversing the object.

In high-energy PRAD with Zumbro lens system, the transmission rate of protons through the object depends on the attenuation and the scattering in the object. The attenuation of protons traversing the object is given by

$$t_\lambda = N/N_0 = e^{-t/\lambda}, \tag{1}$$

where N_0 is the number of the incident protons, N is the number of the protons transmitted through the object, l is area density of the object and λ is the attenuation length of the object. The dependence of attenuation on area density allows the radiography to provide a shadow-graph of area density distribution of the object, which is also the basis of radiography without lens system.

The transmission rate of the Zumbro lens system is mainly caused by the collimator at the Fourier plane and hence depends on scattering angles of the protons. The distribution of the deviation angles caused by MCS is well represented by the Molière theory and is roughly Gaussian

$$f(\theta) = \frac{1}{2\pi\theta_0^2} e^{-\theta^2/2\theta_0^2}, \tag{2}$$

for small angles. The width of the Gaussian distribution from a fit to Molière theory is given by [9]

$$\theta_0 = \frac{13.6}{\beta cp}\sqrt{l/X_0}[1 + 0.038\ln(l/X_0)], \tag{3}$$

where pc and β are proton momentum (in MeV) and relative velocity to light velocity c, and X_0 is the radiation length of the object, of which a parameterization is

$$X_0 = \frac{716.4\,\mathrm{A}}{Z(Z+1)\ln(287/\sqrt{Z})}, \tag{4}$$

in where Z and A are the atomic number and the atomic weight of the material, respectively.

By integrating the angular distribution of Eq. (2) over the lens acceptance, the transmission rate of Zumbro lens system with collimator angle θ_c can be given as

$$\mathtt{t}_X = 2\pi \int_0^{\theta_c} f(\theta)\sin(\theta)\mathrm{d}\theta \approx 1 - e^{-\theta_c^2/2\theta_0^2}. \tag{5}$$

From Eqs. (3) and (4), θ_0 depends on the atomic number Z, so the transmission rate of Zumbro lens system t_X should be correlated to the object material. The total transmission rate of protons is

$$t = t_\lambda t_X. \tag{6}$$

In high-energy PRAD, radiographing the object with a collimator of sufficiently large θ_c so that $t_X \approx 1$, the attenuation rate t_λ can be provided as in the radiography without lens system. Radiographing again with the collimator angle θ_c cutting into the MCS distribution, and comparing the radiograph to the former one, the transmission rate t_X of the collimator angle θ_c can be obtained. The rate t_λ and t_X depend on l/λ and l/X_0, respectively. Since the attenuation length λ and radiation length X_0 have different dependencies on the atomic number, the ability of material identification can be provided.

III. LOW-ENERGY PRAD USING ZUMBRO LENS SYSTEM

The energy dispersion of the protons leaving the object increases with the object thickness. In low-energy PRAD using Zumbro lens system, to lower the chromatic aberration caused by energy dispersion, the object should be of limited thickness. According to the numerical simulation by G4beamline [10], the aluminum foil to be radiographed on the 11 MeV PRAD system should be less than 2.7×10^{-2} g/cm^2 to keep the chromatic blur smaller than 1 mm. This is about three orders of magnitude smaller than the attenuation length of aluminum, so the attenuation of protons passing through the foil object is negligible and the total transmission rate t approximately equals to the transmission rate t_X of the Zumbro lens system.

The transmission rate of Zumbro lens system depends on the MCS angles of the protons. From Eq. (3), the width of distribution of MCS deviation angles increases with the area density l of object. Therefore, under a fixed collimator angle θ_c, the transmission rate t_X in Eq. (5) decreases with increasing area density. If the collimator angle θ_c cuts into the MCS angular distribution, the transmission rate t_X will be sensitive to changes in area density. This correlation between the transmission rate of Zumbro lens system and area density of object allows the low-energy PRAD to provide image contrast, though almost all the probing protons pass through the object.

According to the analysis above, the low-energy PRAD using 11 MeV proton beams is feasible. It can be used to verify the ability of Zumbro lens system for point-to-point focus, and the ability of Fourier plane for selecting the MCS angular range of the protons passing through to the image plane.

Comparing with the high-energy PRAD, the low-energy PRAD has advantages in diagnosing objects of small thicknesses. From Eq. (3) the width of scattering angle distribution is smaller for high-energy protons. For example, the RMS deviation angle θ_0 caused by MCS is 0.23 mrad for 1 GeV protons transmitted through an aluminum foil of area density 2.7×10^{-2} g/cm^2. The deviation angle distribution is so narrow that the protons are hardly blocked off by the collimator (usually with collimator angle θ_c of several mrad according to the design of Zumbro lens system). The transmission rates t_X and t_λ equal to one approximately, so the high-energy PRAD is not able to provide enough contrast of so thin an object. For 11 MeV protons transferring the same aluminum foil, the RMS deviation angle θ_0 is about 15 mrad and the scattering angular distribution can be cut by the collimator angle θ_c of several mrad, thus the low-energy PRAD can provide enough contrast of minor discrepancy of the small area density.

However, since the imaging of low-energy PRAD is independent of proton attenuation in the object and $t_\lambda \approx 1$, the ratio l/λ cannot be provided by low-energy PRAD, neither the material identification.

IV. RESULTS AND DISCUSSION

To verify the technique of Zumbro lens system, an PRAD beamline was built on the 11 MeV proton cyclotron at Institute of Fluid Physics, CAEP. It provides 11 MeV proton beams with average current of 50 μA. As shown in Fig. 1, the proton beams pass through the Φ1 mm pinhole and Al foil diffuser of 20 μm thick to increase the angular divergence. The magnets in the matching section modulated the positions and the angles of protons [7]. The beams arriving at the end of matching section can uniformly illuminate an Φ30 mm area of the object plane and the transverse angles are linearly correlated to the transverse position. At the object plane, protons undergo MCS in the Al foils. The Zumbro lens system transports the protons to the image plane. The scintillator plate at the image plane and the CCD camera record the transverse distribution of protons as a shadow-graph.

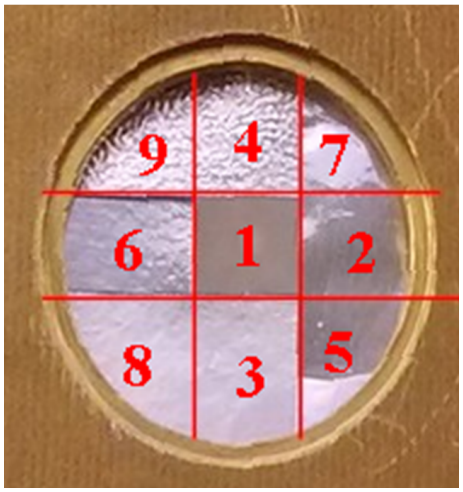

Fig. 4. (Color online) The object made of aluminum foils in a copper support of Φ18 mm. The object had a square hole in the center and eight regions of aluminum foils with different thicknesses. The indexed region numbers correspond to the first column of Table 1.

To measure the transmission rate t_X with the object, transverse distribution of the incident beam was measured. The object was taken away so that the transverse distribution of incident beam at the object plane could be 1 : 1 transferred by the Zumbro lens system to the image plane and recorded by the CCD camera. According to the measurement data, fluctuation of the proton number was less than 2% in tens of hours.

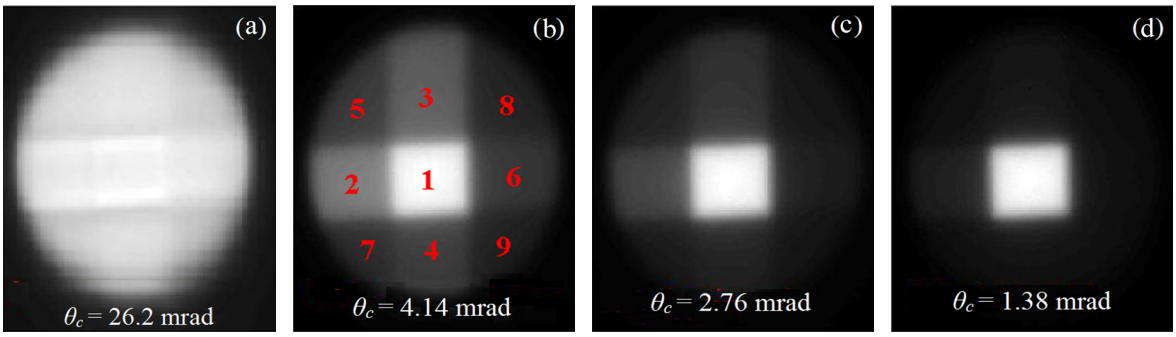

Fig. 5. (Color online) Transmission rate images of the aluminum foil object.

Every time an object was radiographed, the transverse distribution of incident beam was measured again instantly without the object. The transmission rate image was obtained by dividing the radiographic image of the object by the image of the incident beam pixel by pixel.

An object made of aluminum foils was radiographed on the PRAD beamline. As shown in Fig. 4, it has nine regions: the center region is a square hole and the other regions around the hole are aluminum foils of different thicknesses. Table 1 lists the area densities of each region and the corresponding RMS scattering angles of transmitted protons calculated by Eq. (3). The measured transmission rate images with collimator angles θ_c of 26.2, 4.14, 2.76 and 1.38 mrad are shown in Fig. 5.

Figure 5 demonstrates the effects caused by decreased collimator angle. The contrast of the foils with different thicknesses could only be provided when the collimator angle cut into part of the RMS scattering angles θ_0 listed in Table 1. It verified that the Fourier plane is capable of selecting the MCS angular range of the imaging protons.

The transmission rates with collimator angle of 4.14 mrad, which provided good contrast (Fig. 5(b)), were obtained by averaging the measured transmission over a square where the transmission was flat (11 × 11 pixels) for each region in Fig. 5(b). The results were listed in the last column of Table 1. By fitting the measured transmission rates and thicknesses in Table 1 with Eq. (5), the radiation length X_0 of aluminum was 21.3 g/cm^2, being less than the value of 24.3 g/cm^2 calculated by Eq. (4). In Table 1, the measured transmission rates agreed basically with the calculated value. They differ significantly only when the aluminum foil is thinner than 4×10^{-3} g/cm^2. This may due to the contribution of nuclear scattering which is not included in the Gaussian approximation in Eq. (2). The fringe field of the quadrupoles and the nonlinear response of the CCD camera may also affect the measurement.

An aluminum foil covered with charcoal bands was also radiographed. It was in areal density of 2.7×10^{-2} g/cm^2, covered by eight charcoal bands of 1 mm or 2 mm width (four of each). Areal density of the charcoal bands was 6.21×10^{-4} g/cm^2, thus the discrepancy of the area density was about 2.3%. For Al foil of 2.7×10^{-2} g/cm^2 areal density, the RMS deviation angle θ_0 of the traversing protons is about 15 mrad. By setting the collimator angle θ_c of 12.4 mrad, which could cut into the angular distribution, the contrast of the 2.3% area density discrepancy could be provided in the radiographic image (Fig. 6).

TABLE 1. Area densities of the Al foil, and corresponding RMS scattering angle θ_0 and transmission rate t_X of the transmitted protons

Region No.	l (10^{-3} g/cm^2)	θ_0 (mrad)	t_X measured (%) (θ_c = 4.14 mrad)	t_X calculated (%) (θ_c = 4.14 mrad)
1	0(the hole)	0	100	99.92
2	1.656	3.263	55.28	45.33
3	2.475	4.085	40.16	35.49
4	4.080	5.398	25.48	23.44
5	4.131	5.436	25.18	23.05
6	4.324	5.575	24.10	22.19
7	5.736	6.524	18.24	17.87
8	6.799	7.170	15.35	15.65
9	8.404	8.065	12.34	13.28

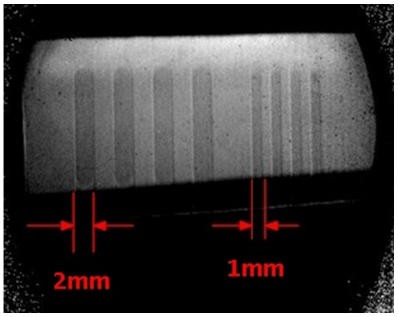

Fig. 6. (Color online) Radiographic image of an aluminum foil covered by eight charcoal bands (with collimator angle of 12.4 mrad).

V. CONCLUSION

According to our analysis, the low-energy PRAD using 11 MeV proton beams could provide shadow-graph of object, though the attenuation of protons in the object was negligible. The imaging contrast of low-energy PRAD is based on the relation between the CMS angular dispersion of the transmitted protons and the thickness of the object.

The experiment on the imaging beamline verified the

point-to-point focus from object to image and the angular sorting of the Fourier plane. The measured transmission rates of aluminum foils agrees with the values calculated from the Gaussian scattering angle distribution for area densities over 4×10^{-3} g/cm^2.

The 11 MeV PRAD system was able to radiograph the object of area density less than 2.7×10^{-2} g/cm^2. By setting the collimator angle cutting into the RMS deviation angle θ_0 of the traversing protons, this low-energy PRAD system could distinguish the area density discrepancy less than 2.3%.

[1] Koehler A. Science, 1968, **160**: 303–304.
[2] Mottershead C T and Zumbro J D. Magnet optics for proton radiography (PAC'97), Vancouver, B. C., Canada, May 12–16, 1997.
[3] King N S P, Ables E, Adams K J, *et al*. Nucl Instrum Meth A, 1999, **424**: 84–91.
[4] Morris C L, Ables E, Alrick K R, *et al*. J Appl Phys, 2011, **109**: 104905.
[5] Ziock H J, Adams K J, Alrick K R, *et al*. The proton radiography concept. Los Alamos National Laboratory, LA-UR-98-1368, 1998.
[6] Burtsev V V, Lebedev A I, Mikhailov A L, *et al*. Combust Explo Shock+, 2011, **47**: 627–638.
[7] Wei T, Yang G J, Li Y D, *et al*. arXiv:1310.5528v1.
[8] He X Z, Yang G J, Long J D, *et al*. Nucl Tech, 2014, **37**: 010201. (in Chinese)
[9] Nakamura K, Hagiwara K, Hikasa K, *et al*. J Phys G Nucl Partic, 2010, **37**: 075021.
[10] http://g4beamline.muonsinc.com.